

Contents lists available at [SciVerse ScienceDirect](http://SciVerse.Sciencedirect.com)

# Journal of Computational and Applied Mathematics

journal homepage: [www.elsevier.com/locate/cam](http://www.elsevier.com/locate/cam)

## Computing steady-state solutions for a free boundary problem modeling tumor growth by Stokes equation

Wenrui Hao<sup>a,\*</sup>, Jonathan D. Hauenstein<sup>b</sup>, Bei Hu<sup>a</sup>, Timothy McCoy<sup>a</sup>, Andrew J. Sommese<sup>a</sup><sup>a</sup> Department of Applied and Computational Mathematics and Statistics, University of Notre Dame, Notre Dame, IN 46556, United States<sup>b</sup> Department of Mathematics, Mailstop 3368, Texas A&M University, College Station, TX 77843, United States

### ARTICLE INFO

#### Article history:

Received 31 October 2011

Received in revised form 6 April 2012

#### Keywords:

Free boundary problems

Stationary solution

Stokes equation

Bifurcation

Homotopy continuation

Tumor growth

### ABSTRACT

We consider a free boundary problem modeling tumor growth where the model equations include a diffusion equation for the nutrient concentration and the Stokes equation for the proliferation of tumor cells. For any positive radius  $R$ , it is known that there exists a unique radially symmetric stationary solution. The proliferation rate  $\mu$  and the cell-to-cell adhesiveness  $\gamma$  are two parameters for characterizing “aggressiveness” of the tumor. We compute symmetry-breaking bifurcation branches of solutions by studying a polynomial discretization of the system. By tracking the discretized system, we numerically verified a sequence of  $\mu/\gamma$  symmetry breaking bifurcation branches. Furthermore, we study the stability of both radially symmetric and radially asymmetric stationary solutions.

© 2012 Elsevier B.V. All rights reserved.

### 1. Introduction

Mathematical models of tumor growth, which consider the tumor tissue as a density of proliferating cells, have been developed and studied in many papers; see [1–9] and their references. These models treat tumor tissue as a porous medium described by Darcy’s law. However, there are tumors for which the tissue is more naturally modeled as a fluid. For example, in the early stages of breast cancer, the tumor is confined to the duct of a mammary gland, which consists of epithelial cells, a meshwork of proteins, and mostly extracellular fluid. Several papers on ductal carcinoma in the breast that use the Stokes equation in their mathematical models are [10–12], which focus on the radially symmetric case since tumors grown in vitro have a nearly spherical shape. It is important to determine whether these radially symmetric tumors are asymptotically stable. While tumors grown in vitro have a nearly spherical shape, tumors grown in vivo are usually not. It is therefore also interesting to study what will happen for the radially asymmetric tumors.

Discretization of a tumor growth model with Stokes equation gives rise to sparse polynomial systems. We use numerical algorithms based on algebraic geometry to solve this free-boundary problem. Over the last decade, numerical algebraic geometry (see [13] for some background), which grew out of continuation methods for finding all isolated solutions of systems of nonlinear multivariate polynomials, has reached a high level of sophistication. The polynomial systems that arise from the discretizations of tumor-growth models [14,15] are many orders of magnitude larger than the polynomial systems that the algorithms of numerical algebraic geometry have been applied to. However, the numerical methods that have been developed are good tools to investigate polynomial systems arising from discretizations of systems of tumor models.

\* Corresponding author.

E-mail addresses: [whao@nd.edu](mailto:whao@nd.edu) (W. Hao), [jhauenst@math.tamu.edu](mailto:jhauenst@math.tamu.edu) (J.D. Hauenstein), [b1hu@nd.edu](mailto:b1hu@nd.edu) (B. Hu), [tmccoy@nd.edu](mailto:tmccoy@nd.edu) (T. McCoy), [sommese@nd.edu](mailto:sommese@nd.edu) (A.J. Sommese).URLs: <http://www.nd.edu/~whao> (W. Hao), <http://www.math.tamu.edu/~jhauenst> (J.D. Hauenstein), <http://www.nd.edu/~b1hu> (B. Hu), <http://www.nd.edu/~sommese> (A.J. Sommese).

In this article, we apply a general numerical algorithmic approach to study a tumor growth model with Stokes equation:

1. numerically compute values of the parameter where bifurcation occurs;
2. numerically compute nonspherical solutions on a branch far from the bifurcation; and
3. determine stability of these solutions.

## 2. Mathematical model

Let  $\Omega(t)$  denote the tumor domain at time  $t$ , and  $p$  be the pressure within the tumor resulting from proliferation of the tumor cells. The density of the cells,  $c$ , depends on the concentration of nutrients,  $\sigma$ , and assuming that this dependence is linear, we may simply identify  $c$  with  $\sigma$ . We also assume the proliferation rate,  $S$ , depends linearly upon  $\sigma$ . That is,

$$\operatorname{div} \vec{v} = S = \mu(\sigma - \tilde{\sigma}) \quad \text{in } \Omega(t), \tag{1}$$

where  $\tilde{\sigma} > 0$  is a threshold concentration,  $\mu$  is the proliferation rate which expresses the “intensity” of the expansion or shrinkage and  $\vec{v}$  is the velocity of the cells moving. The first order Taylor expansion for the fully nonlinear model yields the linear approximation  $\mu(\sigma - \tilde{\sigma})$  used here.

If we assume that the consumption rate of nutrients is proportional to the concentration of the nutrients, then after normalization,  $\sigma$  satisfies

$$\epsilon \sigma_t - \Delta \sigma = -\sigma \quad \text{in } \Omega(t) \quad \text{and} \quad \sigma = 1 \quad \text{on } \partial \Omega(t), \tag{2}$$

where  $\epsilon$  is a small parameter. Most tumor models assume that the tissue has the structure of a porous medium so that Darcy’s law holds. In particular,  $\vec{v} = -\nabla p$  where  $p$  is the pressure. However, the tissue is modeled as a fluid in the current model. In this case, the stress tensor is given by  $\sigma_{ij} = -p\delta_{ij} + 2\nu(e_{ij} - \frac{1}{3}\bar{\Delta}\delta_{ij})$  where  $p = -\frac{1}{3}\sum_{k=1}^3 \sigma_{kk}$ ,  $\nu$  is the viscosity coefficient,  $e_{ij} = \frac{1}{2}(\frac{\partial v_i}{\partial x_j} + \frac{\partial v_j}{\partial x_i})$  is the strain tensor,  $\delta$  is the Kronecker delta and  $\bar{\Delta} = \sum_{k=1}^3 e_{kk} = \operatorname{div} \vec{v}$  is the dilation. If there are no body forces, then  $\sum_{j=1}^3 \frac{\partial \sigma_{ij}}{\partial x_j} = 0$  which can be written as the Stokes equation (see [10–12] for details)

$$-\nu \Delta \vec{v} + \nabla p - \frac{1}{3}\nu \nabla \operatorname{div} \vec{v} = 0 \quad \text{in } \Omega(t), \quad t > 0, \tag{3}$$

where  $\nu$  is a constant and is taken to 1 in our computation for simplicity. Assuming that the strain tensor is continuous up to the boundary of the domain, we then obtain a boundary condition [16]:

$$T(\vec{v}, p)\vec{n} = -\gamma\kappa\vec{n} \quad \text{on } \partial \Omega(t), \quad t > 0, \tag{4}$$

where  $T$  is the stress tensor:  $T(\vec{v}, p) = \nu(\nabla \vec{v} + (\nabla \vec{v})^T) - (p + \frac{2}{3}\nu \operatorname{div} \vec{v})I$  with components

$$T_{ij} = \nu \left( \frac{\partial v_i}{\partial x_j} + \frac{\partial v_j}{\partial x_i} \right) - \delta_{ij} \left( p + \frac{2\nu}{3} \operatorname{div} \vec{v} \right),$$

where  $\vec{n}$  is the outward normal,  $\kappa$  is the mean curvature computed from the shape of the boundary, and  $\gamma$  is the cell-to-cell adhesiveness constant.

The free boundary condition is given by the kinematic condition

$$V_n(t) = \vec{v} \cdot \vec{n} \quad \text{on } \partial \Omega(t). \tag{5}$$

Summarizing these equations, we obtain (see more details in [16])

$$\left\{ \begin{array}{ll} \epsilon \sigma_t - \Delta \sigma + \sigma = 0 & \text{in } \Omega(t) \\ -\Delta \vec{v} + \nabla p = (\mu/3)\nabla(\sigma - \tilde{\sigma}) & \text{in } \Omega(t) \\ \operatorname{div} \vec{v} = \mu(\sigma - \tilde{\sigma}) & \text{in } \Omega(t) \\ T(\vec{v}, p)\vec{n} = \left( -\gamma\kappa + \frac{2\nu}{3}\mu(1 - \tilde{\sigma}) \right) \vec{n} & \text{on } \partial \Omega(t) \\ \sigma = 1 & \text{on } \partial \Omega(t) \\ \vec{v} \cdot \vec{n} = V_n & \text{on } \partial \Omega(t) \\ \int_{\Omega(t)} \vec{v} dx = 0, \quad \int_{\Omega(t)} \vec{v} \times \vec{x} dx = 0 & \end{array} \right. \tag{6}$$

where the last two conditions represent the choice of a coordinate system that excludes the six-dimensional kernel of (1), (3) and (4), which consists of rigid motions.

The steady state fluid-like tumor system is (see more details in [16]):

$$\begin{cases} -\Delta\sigma + \sigma = 0 & \text{in } \Omega \\ -\Delta\vec{v} + \nabla p = (\mu/3)\nabla(\sigma - \tilde{\sigma}) & \text{in } \Omega \\ \operatorname{div}\vec{v} = \mu(\sigma - \tilde{\sigma}) & \text{in } \Omega \\ T(\vec{v}, p)\vec{n} = \left(-\gamma\kappa + \frac{2\nu}{3}\mu(1 - \tilde{\sigma})\right)\vec{n} & \text{on } \partial\Omega \\ \sigma = 1 & \text{on } \partial\Omega \\ \vec{v} \cdot \vec{n} = 0 & \text{on } \partial\Omega \\ \int_{\Omega} \vec{v} dx = 0, \quad \int_{\Omega} \vec{v} \times \vec{x} dx = 0 \end{cases} \quad (7)$$

where  $T(\vec{v}, p)\vec{n} = (\nabla\vec{v})^T + \nabla\vec{v} - pI$  with  $I$  the  $3 \times 3$  identity matrix.

In [16], it is proved that there exists a unique radially symmetric solution with free boundary  $r = R$  for any given positive number  $R$ . For a sequence  $\mu/\gamma = M_n(R)$  there exist symmetry-breaking bifurcation branches of solutions with boundary  $r = R + \epsilon Y_{l,0}(\theta) + O(\epsilon^2)$  ( $n$  even  $\geq 2$ ) for small  $|\epsilon|$ , where  $Y_{n,0}$  is the spherical harmonic of mode  $(n, 0)$ . Note that these results are valid only in a small neighborhood of the bifurcation branching point. In this paper, we use the numerical method presented in [15] to find the radially asymmetric solutions as the parameters *go beyond this small neighborhood*, e.g., Fig. 4. Compared with the system in [15], this system has more variables and increased complexity when using a similar discretization scheme. The comparison of the complexity is shown in Table 1 and thus the extension of our method is not a trivial extension; Due the singular nature of the Jacobian at the bifurcation points, the double precision arithmetic in standard double-precision linear algebra packages such as Matlab had trouble accurately computing these tangent directions. Using multi-precision arithmetic linear algebra, we accurately computed the tangent directions, agreeing with the symbolic formulas. In particular, this large system required us to implement and use parallel differentiation and a sparse linear solver in order to perform the large-scale numerical computations needed for the method developed in [15], which is discussed in Section 4. Just like the system in [15], our numerical bifurcation value matches the theoretical value very well as shown in Table 2.

### 3. Discretization

We use the floating grid mentioned in [14,15] and third order finite difference scheme for the spherical coordinate expression of the radially symmetric stationary solution of system (7) presented in [16]. The formula for the operators in the system in spherical coordinates is deduced in the Appendix. The values  $(\sigma, \vec{v}, p)$  in the small neighborhood of a bifurcation point obtained in [16] via linearization are

$$\begin{cases} \sigma = \sigma_s + \epsilon\sigma_1 + O(\epsilon^2), & \sigma_1 = -(\sigma_s)_r(R) \frac{I_{l+1/2}(r)}{r^{1/2}} \frac{R^{1/2}}{I_{l+1/2}(R)} Y_{l,0}(\theta, \phi) \\ p = p_s + \epsilon p_1 + O(\epsilon^2), & p_1 = \frac{4\mu}{3}\sigma_1 + p_{l,0}(r) Y_{l,0}(\theta, \phi) \\ \vec{v} = \vec{v}_s + \epsilon\vec{v}_1 + O(\epsilon^2), & \vec{v}_1 = \vec{a} + \vec{b} \times \vec{x} + H_1(r) Y_{l,0} \vec{e}_r + H_2(r) \nabla_{\omega} Y_{l,0}(\theta, \phi), \end{cases}$$

where  $Y_{l,0}(\theta, \phi)$  is the spherical harmonic function, which satisfies  $Y_{l,0}(\theta, \phi) = Y_{l,0}(\pi - \theta, \phi)$ ,  $I_{l+1/2}(r)$  is the Modified Bessel function and  $H_1(r)$ ,  $H_2(r)$  are functions of  $r$  (see [16] for detail). Then  $\sigma$  and  $p$  are symmetric with respect to  $\frac{\pi}{2}$ . We note that  $\vec{v}$  can be written as  $v_r \vec{e}_r + v_{\theta} \vec{e}_{\theta} + v_{\phi} \vec{e}_{\phi}$ , that  $\nabla_{\omega} = \frac{1}{\sin(\theta)} \frac{\partial}{\partial\theta} (\sin(\theta) \frac{\partial}{\partial\theta}) + \frac{1}{\sin^2\theta} \frac{\partial^2}{\partial\phi^2}$ , and

$$\begin{cases} \sigma(\theta) = \sigma(\pi - \theta) \\ p(\theta) = p(\pi - \theta) \\ v_r(\theta) = v_r(\pi - \theta) \\ v_{\phi}(\theta) = 0 \\ -v_{\theta}(\theta) = v_{\theta}(\pi - \theta) \end{cases} \quad \text{for } \theta \in \left[0, \frac{\pi}{2}\right]$$

for the bifurcation branch of  $M_n(R)$ , where  $n$  is an even number. In particular, due to this symmetry, we can construct the grid points on one-eighth of the domain and then extend using symmetry to yield solutions to the whole domain.

### 4. Bifurcation of $M_n(R)$

Using the floating grid and third order scheme presented in [14,15], we setup a discretization of the system (7) yielding a polynomial system. Due to the complexity of this polynomial system, it required more computational power than the tumor systems in [14,15]. We used Bertini [17] to handle this polynomial system running on a Xeon 5410 processor using 64-bit Linux. In order to better handle this large-scale problem using Bertini, we implemented parallel differentiation and a sparse linear algebra solver based on BLAS [18] in Bertini. Table 1 compares the number of variables and time needed to track the

**Table 1**  
Comparison of polynomial system solving times.

Tumor model	$N_\theta$	$N_R$	Number of variables	Time
Porous media in [15]	16	30	575	8 min 24 s
	32	60	1135	1 h 30 min
Fluid-like (using sparse linear algebra solver)	16	30	1008	7 h 28 min
	32	60	3938	26 h 34 min

**Table 2**  
Comparison of the numerical values of  $M_n$  with the actual value for a radius of  $R = 12.5$ .

$n$	Formula [16]	Numerical value
$M_4$	0.47481	0.47494
$M_6$	0.47629	0.47702

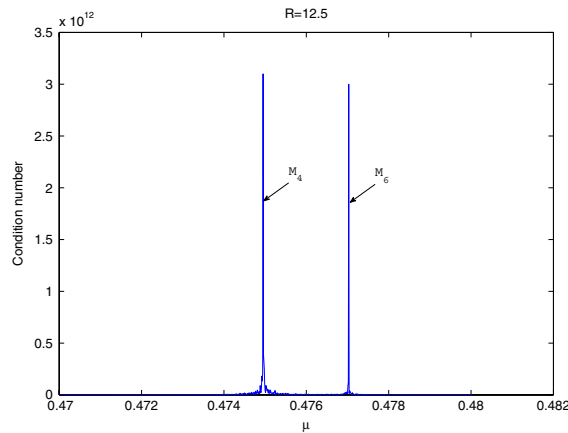


**Fig. 1.** Condition number of the radially symmetric solution vs.  $\mu$ .

discretized polynomial systems along the radially symmetric branch between porous media tumor model and fluid-like tumor model. In this table,  $N_\theta$  and  $N_R$  denote the number of grid points in the angular and radial directions, respectively.

The system is parameterized by  $\mu$  and  $\gamma$ , which characterize the “aggressiveness” of the tumor. It is known [16] that there exists a unique radially symmetric solution with any given  $\mu$ . When we are tracking the radially symmetric solutions along the parameter  $\mu$  with  $\gamma = 1$ , the Jacobian will become singular at  $M_n$  where there exists a bifurcation. Starting from a radially symmetric solution and using parameter continuation with respect to  $\mu$ , we are able to compute the value of  $M_n$  numerically. Fig. 1 plots the condition number of radially symmetric solutions for different  $\mu$  ranging between  $\mu = 0.47$  and  $\mu = 0.48$  with  $R = 12.5$ . We note that there are two bifurcations in the figure, namely  $\mu = M_4$  and  $\mu = M_6$ , respectively. Table 2 compares the numerically computed values of  $M_n$  with the values of  $M_n$  given by the symbolic formulas derived in [16].

The radially asymmetric solutions along the bifurcation branches are even more interesting. We found that the double precision arithmetic in Matlab was unable to accurately compute the tangent directions at  $M_n$ . This stems from the fact that the Jacobian matrix is singular at  $M_n$  and has condition number around  $10^9$  even at values of  $\mu$  where it is nonsingular. By using multi-precision arithmetic [19,20], we were able to compute the tangent directions which agreed with the symbolic formulas derived in [21]. Upon computing the tangent direction, we utilized parameter continuation to track the radially asymmetric solution branches passing through the values of  $M_4$  and  $M_6$  computed above. Fig. 2 shows the solution behavior of these branches which were computed using  $N_R = 60$  grid points in the radial direction and  $N_\theta = 32$  grid points in the angular direction. The function  $\epsilon(\theta)$  in this figure is defined in [15] allowing us to plot the branches. By looking at Fig. 2, we see that there are three intersections. The two intersections, denoted by  $M_U$  and  $M_L$  in Fig. 2 are self-intersections which arise simply by the choice of the projection since the corresponding nonspherical solutions at these points are distinct. The intersection denoted as  $M_{\text{nonspherical}}$  in Fig. 2 is indeed a nonspherical bifurcation. To demonstrate this, Fig. 3 plots the condition number along this path and clearly shows a bifurcation corresponding to the point  $M_{\text{nonspherical}}$ . Fig. 4 plots two nonspherical solutions lying on the  $M_4$  and  $M_6$  branches, respectively. The color at each point represents the value of pressure at this point.

**5. Homotopy continuation of  $M_n$  to  $R$**

For the porous medium tissue model, the smallest value of  $\mu/\gamma$  which generates protrusions is  $M_2(R)$ . At this point, the tumor will have just three protrusions independent of the value of  $R$ . However, in the case of a fluid-like tissue, [21]

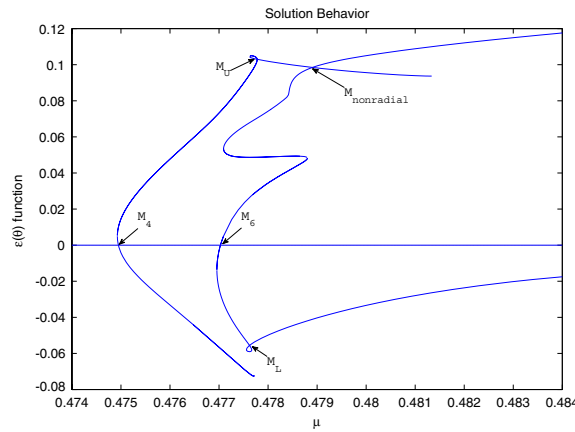


Fig. 2. Solution behavior for  $\gamma = 1$  and  $R = 12.5$ .

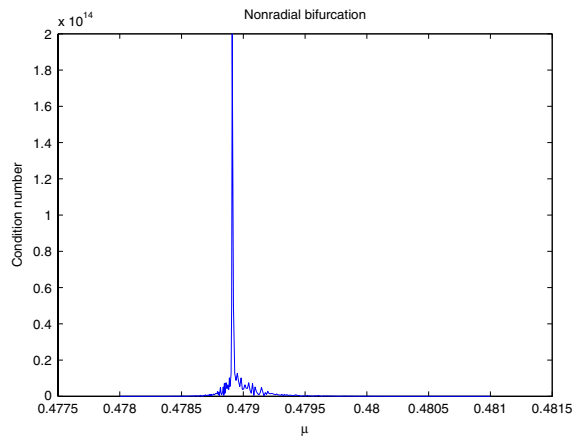


Fig. 3. Nonspherical bifurcation.

shows that the smallest value of  $\mu/\gamma$  which generates protrusions is  $M_{n^*}(R)$ , where  $n^*$  depends on  $R$ . Therefore, one natural question is to determine the values of  $R$  where  $n^*$  changes.

Since the value of  $M_n(R)$  corresponds with a singular solution of a polynomial system, we use deflation [13] to construct a new polynomial system which allows us to track along the path  $M_n(R)$  parameterized by  $R$ . Let  $f(x, \mu)$  denote the discretized polynomial system, where  $x^*$  corresponds to the numerical solution  $(\sigma, p, \vec{v})$  at the bifurcation point  $\mu^*$  of interest. Let  $Jf(x, \mu)$  be the Jacobian matrix of  $f$  at  $x$ . Since the Jacobian is rank deficient, it has nonzero null vectors. One step of the deflation process adds polynomials to  $f$  to yield a general element in this null space, namely the polynomial system

$$g(x, \mu, \xi) = \begin{bmatrix} f(x, \mu) \\ Jf(x, \mu)\xi \\ \mathcal{L}(\xi) \end{bmatrix}$$

where  $\mathcal{L}(\xi)$  is a general linear system so that there is a unique value of  $\xi$  such that  $g(x^*, \mu^*, \xi) = 0$ . Using this augmented polynomial system, we can track a bifurcation value  $M_n$  as  $R$  varies. Fig. 5 plots the value of  $M_4$  with respect to  $R$  along with the numerical error. At the values  $R^*$  where  $n^*$  changes, the solution  $(x, \mu, \xi)$  is singular, that is, the Jacobian matrix of  $g(x, \mu, \xi)$  is rank deficient. Fig. 6 plots the condition number of  $Jg(x, \mu, \xi)$  with respect to  $R$ . This computation yields a numerical value of  $R^* = 12.8778$ .

### 6. Linear stability

We now turn our attention to the numerical determination of solution stability. In order to check linear stability, we rewrite (6) as

$$u_t = F(u, \mu, \tilde{\sigma}, \gamma),$$

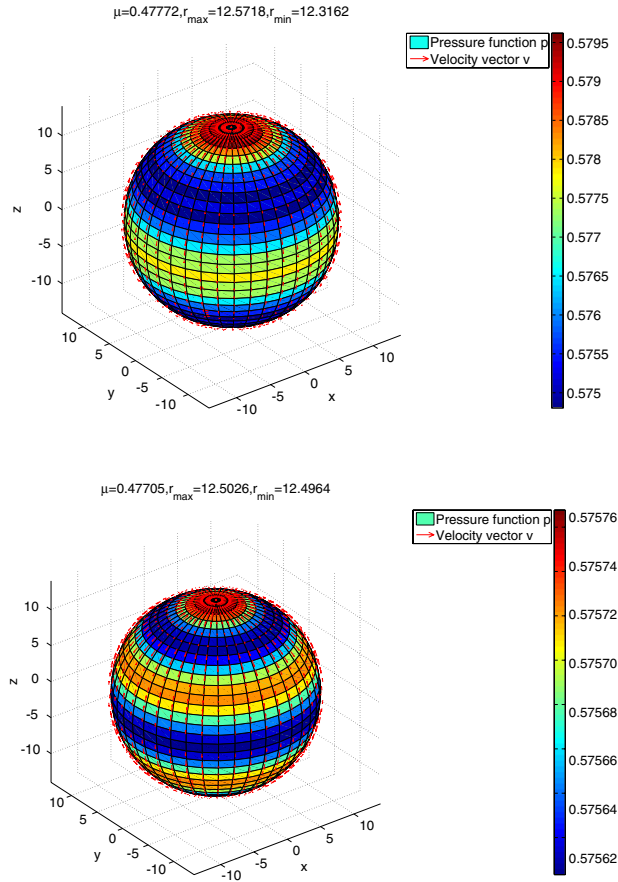


Fig. 4. Nonspherical solutions.

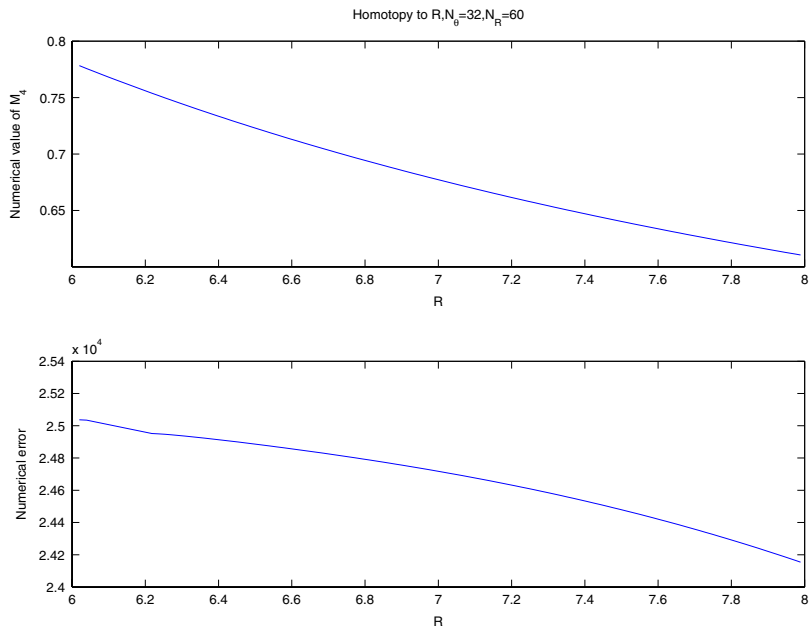


Fig. 5. Homotopy of  $M_4$ .

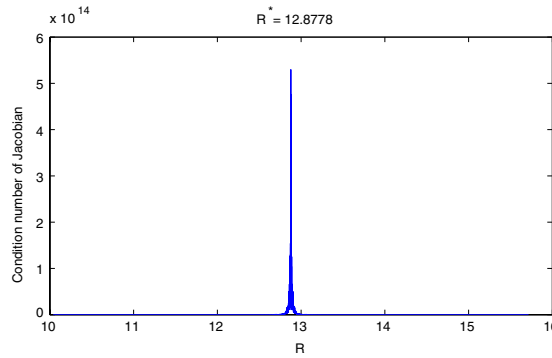


Fig. 6. Condition number of  $Jg(x, \mu, \xi)$  vs.  $R$ .

Table 3  
Maximum eigenvalue for different values of  $\mu$ .

Radial branch		$M_4$ nonspherical branch		$M_6$ nonspherical branch	
$\mu$	$ \rho(A) $	$\mu$	$ \rho(A) $	$\mu$	$ \rho(A) $
1e-2	0.99865	4.75766e-1U	1.00013	4.76956e-1U	1.00013
5e-2	0.99990	4.76641e-1U	1.00026	4.77128e-1U	1.00014
1e-1	0.99999	4.78324e-1U	1.00034	4.77297e-1U	1.00017
2e-1	1.00032	4.79012e-1U	1.00057	4.78802e-1U	1.00024
3e-1	1.00012	4.82764e-1U	1.00106	4.79208e-1U	1.00039
4e-1	1.00049	4.75766e-1L	1.00010	4.77093e-1L	1.00014
5e-1	1.00148	4.76000e-1L	1.00017	4.78053e-1L	1.00267
6e-1	1.00638	4.76290e-1L	1.00022	4.78727e-1L	1.00462
8e-1	1.01846	4.77101e-1L	1.00027	4.82026e-1L	1.00983
1	1.09861	4.77629e-1L	1.00032	4.84000e-1L	1.01472

where  $u = (r, \sigma, p, \bar{v})$ ,  $r$  is the function of the angle  $\theta$  describing the boundary and  $F(u, \mu, \tilde{\sigma}, \gamma)$  represents the steady state system (7). The linearization of the system (6) gives

$$u(t) = u_0 + \epsilon u_1(t) + O(\epsilon^2), \tag{8}$$

where  $u_0$  is the steady state solution. Substituting (8) into (6), we have

$$\begin{aligned} \left( u_0 + \epsilon u_1(t) + O(\epsilon^2) \right)_t &= F(u_0 + \epsilon u_1(t) + O(\epsilon^2), \mu, \tilde{\sigma}, \gamma) \\ &\Rightarrow (u_0)_t + \epsilon (u_1)_t + O(\epsilon^2) = F(u_0, \mu, \tilde{\sigma}, \gamma) + JF(u_0, \mu, \tilde{\sigma}, \gamma)u_1\epsilon + O(\epsilon^2) \\ &\Rightarrow (u_1)_t = JF(u_0, \mu, \tilde{\sigma}, \gamma)u_1, \end{aligned} \tag{9}$$

where  $JF(u_0, \mu, \tilde{\sigma}, \gamma)$  is the Jacobian of  $F(u, \mu, \tilde{\sigma}, \gamma)$  at  $u_0$ . Let  $U_1^n$  denote the numerical approximation of  $u_1(n\tau)$ , where  $\tau$  is the time step size. Then the discretization of (9) leads to

$$U_1^{n+1} = (I - JF(u_0, \mu, \tilde{\sigma}, \gamma)\tau)^{-1}U_1^n \doteq AU_1^n,$$

where  $I$  is the identity matrix. This process transfers the linear stability to the spectrum of  $A$ . Let  $|\rho(A)|$  denote the maximum of the absolute values of the eigenvalues of  $A$ . If  $|\rho(A)| < 1$ , then  $\|U_1^n\| \rightarrow 0$  yielding a stable system. The system is unstable if  $|\rho(A)| > 1$ . Continuing with the working example described in Section 3, namely  $R = 12.5$ , we computed the eigenvalues of  $A$  for different values of  $\mu$  along the radially asymmetric solution branches to determine the stability which are displayed in Table 3. We note that “U” and “L” represent the “upper” and “lower” branches, respectively.

Table 3 shows that the solution is unstable even before the parameter  $\mu$  reaches its first bifurcation point. This is in contrast with tumors growing in porous media environment where spherical instability occurs only when  $\mu$  reaches the first bifurcation point. Moreover, all of the nonspherical solutions computed are unstable while there are some stable nonspherical solutions for a porous tumor [15].

### 7. Conclusion

In this paper, we applied numerical algebraic geometry methods to compute steady states of tumor growth with Stokes equation. The tumor model we considered is a free boundary model with bifurcation phenomenon. The difficulty level of this problem is due to large scale computation magnitude. By implementing parallel differentiation and sparse homotopy tracking with multi-precision arithmetic, we can compute the bifurcation point numerically and track the bifurcation

branches more efficiently. These tools are general numerical algorithmic approaches that can be applied to other large scale polynomial systems.

The model discussed in this article has incorporated important physical quantities such as internal tumor pressure and cell-to-cell adhesion. The bifurcation diagram, which was drawn using homotopy tracking, shows the local behavior of the steady state solutions. Although the tumor model analyzed here is quite simple, this work provides a possible way to study the behavior of the tumor as the parameter changes. In early results, bifurcation theory was used to analyze the bifurcation branch, but only in a small neighborhood of the bifurcation point. In reality, tumor in vivo is unlikely to be of spherical shape. Thus, our tracking along the nonspherical bifurcation branch in this paper may provide significant application.

**Acknowledgments**

The authors would like to thank the Notre Dame Center for Research Computing (crc.nd.edu) for their help; not only for helping maintain our group’s computer cluster, but also for providing access to a high memory node during the period when we were parallelizing the differentiation code in Bertini.

Wenrui Hao was supported by the Dunces Chair of the University of Notre Dame and NSF grant DMS-0712910. Jonathan D. Hauenstein was supported by Texas A&M University and NSF grant DMS-0915211 and DMS-1114336. Andrew J. Sommese was supported by the Duncan Chair of the University of Notre Dame and NSF grant DMS-0712910.

**Appendix. Operators under the spherical coordinate**

We use the notation  $\vec{e}_r, \vec{e}_\theta, \vec{e}_\phi$  for the unit normal vectors in the  $r, \theta, \phi$  directions, respectively; here  $0 \leq r \leq \infty, 0 \leq \theta \leq \pi, 0 \leq \phi \leq 2\pi$ . Then, written in Cartesian coordinates in  $\mathbb{R}^3$ ,

$$\begin{aligned} \vec{e}_r &= \vec{e}_1 \sin \theta \cos \phi + \vec{e}_2 \sin \theta \sin \phi + \vec{e}_3 \cos \theta, \\ \vec{e}_\theta &= \vec{e}_1 \cos \theta \cos \phi + \vec{e}_2 \sin \theta \sin \phi + \vec{e}_3 \cos \theta, \\ \vec{e}_\phi &= -\vec{e}_1 \sin \phi + \vec{e}_2 \cos \phi, \end{aligned}$$

where  $(\vec{e}_1, \vec{e}_2, \vec{e}_3)$  is the standard basis in  $\mathbb{R}^3$  in Cartesian coordinates.

The gradient of the vector  $\nabla \vec{v}$ , where  $\vec{v} = (v_r, v_\theta, v_\phi)^T = v_r \vec{e}_r + v_\theta \vec{e}_\theta + v_\phi \vec{e}_\phi$ , is given by

$$\nabla \vec{v} = \nabla v_r \otimes \vec{e}_r + \nabla v_\theta \otimes \vec{e}_\theta + \nabla v_\phi \otimes \vec{e}_\phi + v_r \nabla \vec{e}_r + v_\theta \nabla \vec{e}_\theta + v_\phi \nabla \vec{e}_\phi. \tag{10}$$

In polar spherical coordinates, the gradient of a function  $f$  has the following form:

$$\nabla f = \frac{\partial f}{\partial r} \vec{e}_r + \frac{1}{r \sin \theta} \frac{\partial f}{\partial \phi} \vec{e}_\phi + \frac{1}{r} \frac{\partial f}{\partial \theta} \vec{e}_\theta.$$

Then, we can deduce the each term of (10) as follows,

$$\begin{aligned} \nabla v_r \otimes \vec{e}_r &= \left( \frac{\partial v_r}{\partial r} \vec{e}_r + \frac{1}{r \sin \theta} \frac{\partial v_r}{\partial \phi} \vec{e}_\phi + \frac{1}{r} \frac{\partial v_r}{\partial \theta} \vec{e}_\theta \right) \otimes \vec{e}_r \\ &= \frac{\partial v_r}{\partial r} \vec{e}_r \otimes \vec{e}_r + \frac{1}{r \sin \theta} \frac{\partial v_r}{\partial \phi} \vec{e}_\phi \otimes \vec{e}_r + \frac{1}{r} \frac{\partial v_r}{\partial \theta} \vec{e}_\theta \otimes \vec{e}_r \\ \nabla v_\theta \otimes \vec{e}_\theta &= \frac{\partial v_\theta}{\partial r} \vec{e}_r \otimes \vec{e}_\theta + \frac{1}{r \sin \theta} \frac{\partial v_\theta}{\partial \phi} \vec{e}_\phi \otimes \vec{e}_\theta + \frac{1}{r} \frac{\partial v_\theta}{\partial \theta} \vec{e}_\theta \otimes \vec{e}_\theta \\ \nabla v_\phi \otimes \vec{e}_\phi &= \frac{\partial v_\phi}{\partial r} \vec{e}_r \otimes \vec{e}_\phi + \frac{1}{r \sin \theta} \frac{\partial v_\phi}{\partial \phi} \vec{e}_\phi \otimes \vec{e}_\phi + \frac{1}{r} \frac{\partial v_\phi}{\partial \theta} \vec{e}_\theta \otimes \vec{e}_\phi \\ v_r \nabla \vec{e}_r &= v_r \left( \frac{\partial \vec{e}_r}{\partial r} \vec{e}_r + \frac{1}{r \sin \theta} \frac{\partial \vec{e}_r}{\partial \phi} \vec{e}_\phi + \frac{1}{r} \frac{\partial \vec{e}_r}{\partial \theta} \vec{e}_\theta \right) \\ &= \frac{v_r}{r} (\vec{e}_\phi \otimes \vec{e}_\phi + \vec{e}_\theta \otimes \vec{e}_\theta) \\ v_\theta \nabla \vec{e}_\theta &= \frac{v_\theta}{r} (\cot \theta \vec{e}_\phi \otimes \vec{e}_\phi - \vec{e}_r \otimes \vec{e}_\theta) \\ v_\phi \nabla \vec{e}_\phi &= -\frac{v_\phi}{r} (\cot \theta \vec{e}_\theta \otimes \vec{e}_\phi + \vec{e}_r \otimes \vec{e}_\phi). \end{aligned}$$

Therefore, we summarize the gradient of velocity as

$$\nabla \vec{v} = \begin{pmatrix} \frac{\partial v_r}{\partial r}, & \frac{1}{r} \frac{\partial v_r}{\partial \theta}, & \frac{1}{r \sin \theta} \frac{\partial v_r}{\partial \phi} \\ \frac{\partial v_\theta}{\partial r} - \frac{v_\theta}{r}, & \frac{1}{r} \frac{\partial v_\theta}{\partial \theta} + \frac{v_r}{r}, & \frac{1}{r \sin \theta} \frac{\partial v_\theta}{\partial \phi} \\ \frac{\partial v_\phi}{\partial r} - \frac{v_\phi}{r}, & \frac{1}{r} \frac{\partial v_\phi}{\partial \theta} - \frac{\cot \theta}{r} v_\phi, & \frac{1}{r \sin \theta} \frac{\partial v_\phi}{\partial \phi} + \frac{v_r}{r} + \frac{\cot \theta}{r} v_\theta \end{pmatrix}.$$



A vector Laplacian can be defined for a vector  $\vec{v}$  by

$$\Delta \vec{v} = \nabla(\nabla \cdot \vec{v}) - \nabla \times (\nabla \times \vec{v}).$$

Moreover, the curl  $\nabla \times \vec{v}$  under spherical coordinates is given by

$$\nabla \times \vec{v} = \frac{\vec{e}_r}{r \sin \theta} \left[ \frac{\partial}{\partial \theta} (v_\phi \sin \theta) - \frac{\partial v_\theta}{\partial \phi} \right] + \frac{\vec{e}_\theta}{r \sin \theta} \left[ \frac{\partial v_r}{\partial \phi} - \sin \theta \frac{\partial}{\partial r} (r v_\phi) \right] + \frac{\vec{e}_\phi}{r} \left[ \frac{\partial}{\partial r} (r v_\theta) - \frac{\partial v_r}{\partial \theta} \right].$$

Thus, the Laplacian of velocity can be expressed as

$$\Delta \vec{v} = \begin{pmatrix} \frac{1}{r} \frac{\partial^2 (r v_r)}{\partial r^2} + \frac{1}{r^2} \frac{\partial^2 v_r}{\partial \theta^2} + \frac{1}{r^2 \sin^2 \theta} \frac{\partial^2 v_r}{\partial \phi^2} + \frac{\cot \theta}{r^2} \frac{\partial v_r}{\partial \theta} - \frac{2}{r^2} \frac{\partial v_\theta}{\partial \theta} - \frac{2}{r^2 \sin \theta} \frac{\partial v_\phi}{\partial \phi} - \frac{2 v_r}{r^2} - \frac{2 \cot \theta}{r^2} v_\theta \\ \frac{1}{r} \frac{\partial^2 (r v_\theta)}{\partial r^2} + \frac{1}{r^2} \frac{\partial^2 v_\theta}{\partial \theta^2} + \frac{1}{r^2 \sin^2 \theta} \frac{\partial^2 v_\theta}{\partial \phi^2} + \frac{\cot \theta}{r^2} \frac{\partial v_\theta}{\partial \theta} - \frac{2 \cot \theta}{r^2 \sin \theta} \frac{\partial v_\phi}{\partial \phi} + \frac{2}{r^2} \frac{\partial v_r}{\partial \theta} - \frac{1}{r^2 \sin^2 \theta} v_\theta \\ \frac{1}{r} \frac{\partial^2 (r v_\phi)}{\partial r^2} + \frac{1}{r^2} \frac{\partial^2 v_\phi}{\partial \theta^2} + \frac{1}{r^2 \sin^2 \theta} \frac{\partial^2 v_\phi}{\partial \phi^2} + \frac{\cot \theta}{r^2} \frac{\partial v_\phi}{\partial \theta} + \frac{2}{r^2 \sin \theta} \frac{\partial v_r}{\partial \phi} + \frac{2 \cot \theta}{r^2 \sin \theta} \frac{\partial v_\theta}{\partial \phi} - \frac{1}{r^2 \sin^2 \theta} v_\phi \end{pmatrix}.$$

## References

- [1] J.A. Adam, S.A. Maggelakis, Diffusion regulated growth characteristics of a spherical prevascular carcinoma, *Bull. Math. Biol.* 52 (1990) 549–582.
- [2] N. Britton, M.A.J. Chaplain, A qualitative analysis of some models of tissue growth, *Math. Biosci.* 113 (1993) 77–89.
- [3] H.M. Byrne, The importance of intercellular adhesion in the development of carcinomas, *IMA J. Math. Appl. Med. Biol.* 14 (1997) 305–323.
- [4] H.M. Byrne, A weakly nonlinear analysis of a model of avascular solid tumor growth, *J. Math. Biol.* 39 (1999) 59–89.
- [5] H.M. Byrne, M.A.J. Chaplain, Growth of nonnecrotic tumors in the presence and absence of inhibitors, *Math. Biosci.* 130 (1995) 151–181.
- [6] H.M. Byrne, M.A.J. Chaplain, Modelling the role of cell–cell adhesion in the growth and development of carcinomas, *Math. Comput. Modelling* 12 (1996) 1–17.
- [7] M.A.J. Chaplain, The development of a spatial pattern in a model for cancer growth, in: H.G. Othmer, P.K. Maini, J.D. Murray (Eds.), *Experimental and Theoretical Advances in Biological Pattern Formation*, Plenum Press, 1993, pp. 45–60.
- [8] H.P. Greenspan, On the growth of cell culture and solid tumors, *J. Theoret. Biol.* 56 (1976) 229–242.
- [9] D.L.S. McEwain, L.E. Morris, Apoptosis as a volume loss mechanism in mathematical models of solid tumor growth, *Math. Biosci.* 39 (1978) 147–157.
- [10] S.J.H. Franks, H.M. Byrne, J.C.E. Underwood, C.E. Lewis, Biological inferences from a mathematical model of comedo ductal carcinoma in situ of the breast, *J. Theoret. Biol.* 232 (2005) 523–543.
- [11] S.J.H. Franks, H.M. Byrne, J.P. King, J.C.E. Underwood, C.E. Lewis, Modelling the early growth of ductal carcinoma in situ of the breast, *J. Math. Biol.* 47 (2003) 424–452.
- [12] S.J.H. Franks, H.M. Byrne, J.P. King, J.C.E. Underwood, C.E. Lewis, Modelling the growth of ductal carcinoma in situ, *Math. Med. Biol.* 20 (2003) 277–308.
- [13] A.J. Sommese, C.W. Wampler, *The Numerical Solution of Systems of Polynomials Arising in Engineering and Science*, World Scientific Publishing Co. Pvt. Ltd., Hackensack, NJ, 2005.
- [14] W. Hao, J.D. Hauenstein, B. Hu, Y. Liu, A.J. Sommese, Y.-T. Zhang, Bifurcation for a free boundary problem modeling the growth of a tumor with a necrotic core, *Nonlinear Anal. RWA* 13 (2012) 694–709.
- [15] W. Hao, J.D. Hauenstein, B. Hu, A.J. Sommese, A three-dimensional steady-state tumor system, *Appl. Math. Comput.* 218 (2011) 2661–2669.
- [16] A. Friedman, B. Hu, Bifurcation for a free boundary problem modeling tumor growth by Stokes equation, *SIAM J. Math. Anal.* 30 (1) (2006) 174–194.
- [17] D.J. Bates, J.D. Hauenstein, A.J. Sommese, C.W. Wampler, Bertini: software for numerical algebraic geometry. Available at: [www.nd.edu/~sommese/bertini](http://www.nd.edu/~sommese/bertini).
- [18] Sparse basic linear algebra subprograms (BLAS) library. <http://math.nist.gov/spblas/>.
- [19] D.J. Bates, J.D. Hauenstein, A.J. Sommese, C.W. Wampler, Adaptive multiprecision path tracking, *SIAM J. Numer. Anal.* 46 (2008) 722–746.
- [20] D.J. Bates, J.D. Hauenstein, A.J. Sommese, C.W. Wampler, Stepsize control for adaptive multiprecision path tracking, in: D. Bates, G. Besana, S. Di Rocco, C. Wampler (Eds.), *Interactions of Classical and Numerical Algebraic Geometry*, in: *Contemporary Mathematics*, 2009.
- [21] A. Friedman, B. Hu, Bifurcation from stability to instability for a free boundary problem modeling tumor growth by Stokes equation, *J. Math. Anal. Appl.* 207 (2007) 643–664.